INSTITUTE OF PHYSICS PUBLISHING JOURNAL OF PHYSICS: CONDENSED MATTER

J. Phys.: Condens. Matter **18** (2006) 8367–8381 doi:10.1088/0953-8984/18/35/021

Ab initio calculations of the BaF_2 bulk and surface F centres

H Shi[1], **R I Eglitis and G Borstel**

Fachbereich Physik, Universität Osnabrück, D-49069 Osnabrück, Germany

E-mail: hshi@uos.de

Received 22 May 2006, in final form 27 July 2006
Published 18 August 2006
Online at stacks.iop.org/JPhysCM/18/8367

Abstract

A hybrid Hartree–Fock and density functional theory, in which Hartree–Fock exchange is mixed with density functional theory exchange functionals, using Beckes' three-parameter method, combined with the non-local correlation functionals by Perdew and Wang, allows us to achieve the best agreement with experiment (11.00 eV) for the BaF_2 band gap (11.30 eV). The characterization of F centres in BaF_2 is still a question of debate. In order to understand the behaviour of the material, we performed *ab initio* calculations to determine their electronic structure, atomic geometry and formation energy. We also calculated the M centre, the simplest aggregation of two F centres, and the results show that the β band absorption in BaF_2 is predominantly due to the presence of M centres.

(Some figures in this article are in colour only in the electronic version)

1. Introduction

Despite the fact that BaF_2 has enough technological potential, there has not been much theoretical work carried out. BaF_2 is an important member of the alkali earth fluorides and has been studied for its intrinsic optical properties [1–4]. These optical properties are related to the structural and electronic properties of BaF_2, such as a very large band gap. The energy-gap width between valence and conduction bands at the Γ point in BaF_2 according to *ab initio* calculations performed by means of the full-potential linearized augmented plane-wave (FPLAPW) method, as implemented in the WIEN-97 code [5], is 7.49 eV, considerably less than the experimental value of 11.00 eV [6]. BaF_2 is also the fastest luminescent material that has been found to date [7]. Recently, BaF_2 has also been found to exhibit superionic conductivity by dissolving appropriate impurities into the lattice or by introducing an interface that causes the redistribution of ions in the space charge region, and is therefore considered as a candidate material for high-temperature batteries, fuel cells, chemical filters and sensors [8].

[1] Author to whom any correspondence should be addressed.

Arends [9] discovered the paramagnetic resonance of F centres in additively coloured BaF_2. This defect is an electron trapped in an anion vacancy which is created on removal of the anion by irradiation or by additive colouration. The electron-nuclear double resonance (ENDOR) measurements of Hayes and Stott [10] and Stoneham *et al* [11] have confirmed the results of the electron paramagnetic resonance (EPR) method for BaF_2. Theoretical study of F centres in BaF_2 based on a quantum molecular cluster embedded in a classical crystal was performed by Vail *et al* [12]. Their work is initial research on a diffuse excited electronic state of the F centre. Accordingly, other computational details of the F centres in BaF_2 are not included in their paper. Recently, nominally pure BaF_2 crystals were investigated at 77 K with optical absorption and EPR to understand the mechanism of radiation damage. Nepomnyashchikh *et al* [4] measured that x-ray irradiation at 77 K of undoped BaF_2 produces V_k and F centres having absorption bands at 3.4 and 2.3 eV, respectively. The V_k centre is formed when a hole is trapped by the fluorine ion in BaF_2 crystal.

The characterization of F centres in BaF_2 has important technological implications, but it appears that the electronic structure of F centres is far from being understood, even from a qualitative point of view. In this paper, we performed *ab initio* calculations to determine their electronic structure, atomic geometry and formation energy. To get a reliable basis for defect calculations, which firstly requires a precise description of the band gap, we calculated the electronic structure of BaF_2 bulk. In a second part of the paper, we present theoretical investigations for pure BaF_2(111), (110), (100) surfaces and F centres therein.

2. Method of calculations

To perform the first-principles DFT-B3PW calculations, we used the CRYSTAL2003 computer code [13]. This code employs Gaussian-type functions (GTF) localized at atoms as the basis for an expansion of the crystalline orbitals. Features of the CRYSTAL2003 code, which are most important for this study, are its ability to calculate the electronic structure of materials within both Hartree–Fock and Kohn–Sham (KS) Hamiltonians. However, in order to employ the LCAO-GTF (linear combination of atomic orbitals) method, it is desirable to have optimized basis sets (BS). Such BS optimization for $BaTiO_3$ perovskite was developed and discussed in [14, 15]. The Hay–Wadt small-core effective core pseudopotential (ECP) was adopted for the Ba atom [16]. The small-core ECP replaces only inner core orbitals, but orbitals for sub-valence electrons as well as for valence electrons are calculated self-consistently. In the present paper, we used this new BS for the Ba atom. The basis sets are believed to be transferable, so that, once determined for some chemical constituent, they may be applied successfully in the calculations for a variety of chemical substances where the latter participates. Besides giving a reasonable lattice constant [14], our basis set for Ba also allowed us to achieve excellent results for $BaTiO_3$(001) surface relaxation and the surface band structure [15]. For the F atom we used the same basis set as in our previous paper, dealing with the CaF_2 electronic structure and F centres therein [17].

In our calculations, we used a hybrid Hartree–Fock (HF) and density functional theory (DFT) exchange functional, in which HF exchange is mixed with DFT exchange functionals, using Beckes' three-parameter method [18], combined with the non-local correlation functionals by Perdew and Wang (B3PW) [19–21]. It is well known that the HF method considerably overestimates the optical band gap and DFT underestimates it, but the B3PW method, as shown in our previous calculations, allows us to achieve excellent agreement with the experimental band gap [1, 14, 15]. The reciprocal space integration was performed by sampling the Brillouin zone of the unit cell with the $8\times8\times8$ Pack–Monkhorst net [22]. Another advantage of the CRYSTAL2003 code is its treatment of purely two-dimensional slabs, without

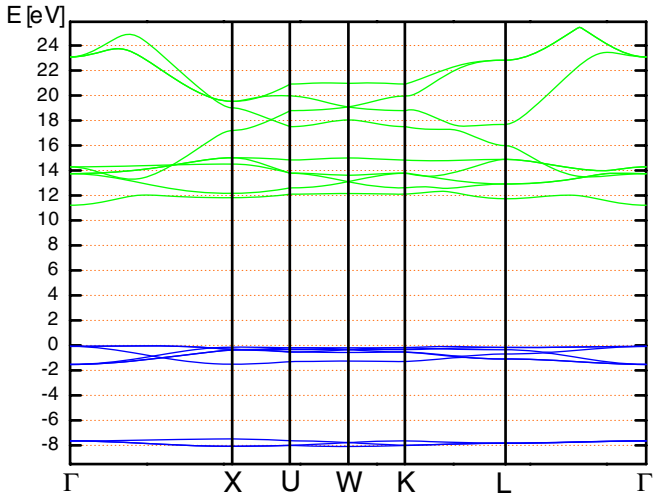

Figure 1. Electronic band structure of BaF_2 bulk calculated by means of the hybrid B3PW method.

artificial periodicity in the direction perpendicular to the surface, commonly employed in most other surface calculations [23, 24].

To simulate F centres, we started with a 48-atom supercell with one of the fluorine atoms removed. After the fluorine atom is removed, the atomic configuration of the surrounding atoms is re-optimized via a search for the total energy minimum as a function of the atomic displacements from the regular lattice sites. In order to have an accurate description of the F centre, a basis set has been added at the fluorine vacancy, corresponding to the *ghost* atom [17]. For the *ghost* atom, we used the same basis set as that used for the F^- ions of the bulk BaF_2. For the M centre system, we used a 96-atom supercell with two of the neighbour fluorine atoms removed. It is found that rather limited basis sets are enough to predict excitation energies of the F and F^+ centres in MgO [25] that are near to each other, as is observed experimentally.

3. BaF_2 bulk and surface electronic structure

As a starting point for our calculations, we calculated the BaF_2 lattice constant (6.26 Å) and bulk modulus (61 GPa). Our results are in good agreement with the experimental data for the lattice constant (6.20 Å) and the bulk modulus (57 GPa) [26]. The Ba and F effective charges (obtained using the Mulliken population analysis) ($+1.845e$ and $-0.923e$, respectively) are very close to those expected in an ionic model ($+2e$ and $-1e$, respectively). The F–F bond population ($-2me$) is close to zero and the F–Ba bond population ($-38me$) is even negative, which indicates repulsion.

Experimentally, the direct band gap ($\Gamma \rightarrow \Gamma$) for BaF_2 bulk is 11.00 eV [6]. Our calculated (see figure 1) band gap for BaF_2 by means of B3PW method (11.30 eV) is in much better agreement with experiment, such as the recent result of Khenata *et al* (7.49 eV) using the FPLAPW method [5]. Our result for the BaF_2 band gap is in a line with the early conclusion by Muscat *et al* [27] that the hybrid scheme allows us to achieve the best agreement with experiment for the band gaps of a variety of materials.

We calculated the surface energetics using the following equation:

$$E_{\text{surface}} = \tfrac{1}{2}[E_{\text{slab}}^{(\text{relax})} - nE_{\text{bulk}}] \tag{1}$$

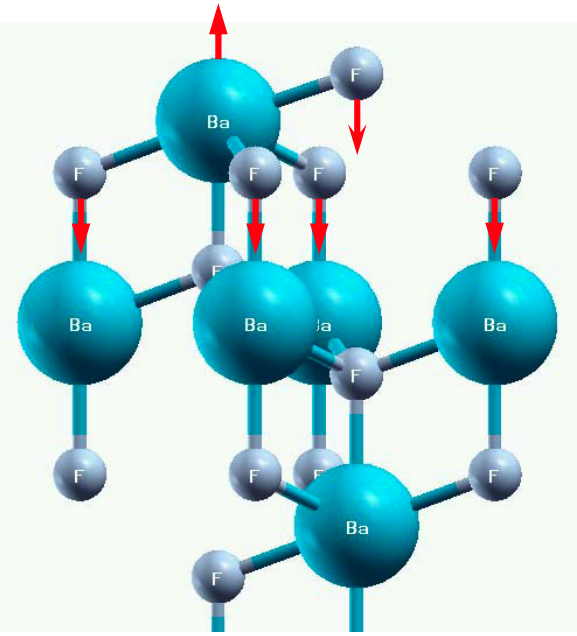

Figure 2. Schematic sketch of $BaF_2(111)$ surface structure. Arrows indicate the calculated displacement directions of Ba and F atoms.

where n is the number of bulk primitive cells in the slab. E_{bulk} is the total energy per bulk unit cell, and $E_{\text{slab}}^{(\text{relax})}$ is the total energy for a relaxed slab containing n layers. According to the results of our calculations, using the slab containing 15 layers, the $BaF_2(111)$ surface (0.334 J m^{-2}) is the most stable one. Our calculated surface energy for the (110) surface is considerably larger (0.494 J m^{-2}) than for the (111) surface. Finally, our calculations show that the surface energy for the (100) surface is the largest one (0.666 J m^{-2}). We also calculated the surface energies for these three cases containing 13 and 17 layers, respectively, and the results show that the surface energies do not change. According to our knowledge, there are no experimental data dealing with surface energies of BaF_2. In comparison with our previous calculations for CaF_2, we predict that the $BaF_2(111)$ surface (0.334 J m^{-2}) is slightly more stable than the $CaF_2(111)$ surface (0.438 J m^{-2}) [17].

The structure of the $BaF_2(111)$ surface and the directions of atomic displacements are illustrated in figure 2. The calculated atomic displacements in the upper three layers (nine sublayers) are listed in table 1. According to our calculations, the relaxation of F atoms in the upper sublayer of the top (111) surface layer is inward by 0.054 Å, and is comparable with experiment (0.12 $\pm$ 0.07 Å) [28], which investigated the $BaF_2(111)$ surface by means of low-energy electron diffraction (LEED). The experiment also shows that the positions of Ba atoms, as well as those of the second fluoride sublayer in this topmost F–Ba–F sheet, are almost identical to their bulk values. Our results of the displacements of Ba atoms and lower F atoms in the topmost F–Ba–F layer are in agreement with this experiment. The surface-layer relaxation of F atoms in the BaF_2 upper sublayer has the same direction and comparable magnitude as we found earlier for CaF_2 [17].

We also calculated the geometry relaxation for the (110) and (100) slabs. For the (110) surface, Ba atoms in the top layer move inward (towards the bulk) by 3.15% of the lattice

Table 1. Atomic relaxation of a BaF_2 slab in (111) direction (as a percentage of the lattice constant), calculated by means of the hybrid B3PW method. Positive signs correspond to outward atomic displacements (toward the vacuum).

Layer	Atom	ΔZ (a_0 %)
1	F	−0.87
	Ba	+0.17
	F	−0.37
2	F	+0.73
	Ba	+0.19
	F	−0.07
3	F	+0.25
	Ba	+0.01
	F	−0.15

Table 2. The calculated direct ($\Gamma \rightarrow \Gamma$) optical gap (in eV) for the BaF_2(111), (110) and (100) slabs. All calculations have been performed using the hybrid B3PW method.

BaF_2 slabs	(111)	(110)	(100)	BaF_2 bulk
$\Gamma \rightarrow \Gamma$ optical gap (eV)	10.94	10.77	10.29	11.30

constant a_0, whereas the displacement of upper layer Ba atoms in the case of BaF_2(111) termination was only 0.17% of a_0 (see table 1) backwards from the bulk. Also, for the deeper layers, the magnitudes of the atomic displacements in the case of the (110) surface are considerably larger than for the (111) surface. For the (100) case, F atoms in the top layer are relaxed most noticeably, by 6.53% of a_0 towards the bulk. According to our calculations, we found that the relaxation of (100) surface is considerably stronger than for the (111) and (110) surfaces.

The cation effective charges in the top BaF_2(111) surface layer ($+1.838e$) turn out to be smaller than in the bulk ($+1.845e$), whereas the F charges ($-0.918e$) in the upper sublayer of the top surface layer are larger by $0.005e$ than in the bulk ($-0.923e$). Changes in the atomic charges in the deeper layers become very small. The charge of the (110) surface top layer fluorine atoms is $-0.908e$, and increases by $0.015e$ in comparison to the bulk, and by $0.010e$ relative to the (111) surface top layer fluorine atoms. The largest change in charge is for the BaF_2(110) surface top layer Ba atoms. Their charge is reduced by $0.042e$ in comparison to the bulk charge ($+1.845e$) and is equal to $+1.803e$. Charges in deeper (110) slab layers become very close to the relevant Ba and F charges in the bulk. Static Mulliken charges of atoms for the BaF_2(100) surface differ from the bulk charges by $+0.047e$ for the F in the top layer and by $-0.051e$ for the Ba in the second layer, which is considerably more than in the cases of (111) and (110) surfaces.

We also computed the electronic energy band structures for the BaF_2(111), (110) and (100) surfaces. As we can see from the main results collected in table 2, the direct optical band gap for the (111) surface (10.94 eV) (see figure 3) is closer to the relevant optical band gap value for the BaF_2 bulk (11.30 eV) than that of the (110) surface (10.77 eV). The direct optical band gap for the BaF_2(100) surface (10.29 eV) is considerably reduced in comparison to the BaF_2 bulk. We also found a similar effect, reduction of the (100) surface band structure, for ABO_3 perovskites [15].

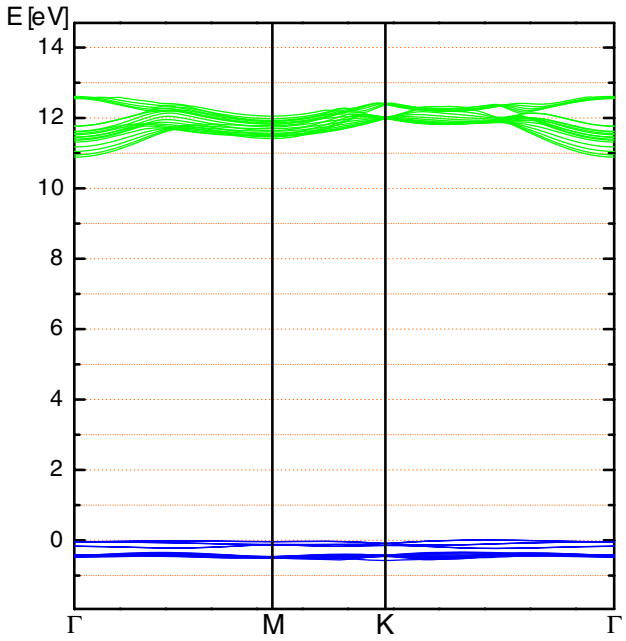

Figure 3. Electronic band structure of $BaF_2(111)$ surface calculated by means of the hybrid B3PW method.

4. F centre in BaF_2

To estimate the formation energy of the fluorine vacancy in BaF_2 crystal, we used the following expression [29–31]:

$$E_{\text{formation}} = E(\text{fluorine}) + E(\text{F}) - E(\text{perfect}) \tag{2}$$

where $E(\text{fluorine})$ is the energy for the isolated fluorine atom, and $E(\text{F})$ and $E(\text{perfect})$ are the energies of the defective crystal containing the F centre and the perfect crystal, respectively. The vacancy formation energy is independent of the system size and, according to our calculations by means of the hybrid B3PW functional, equal to 7.82 eV for supercells containing 12, 24 and 48 atoms.

The redistribution of the electrons after vacancy formation can be seen in figure 4 for a supercell containing 48 atoms. The analysis of the effective charges shows that the electron associated with the removed F atom is well localized ($-0.801e$) inside the fluorine vacancy (V_F), $-0.068e$ is localized on the four nearest Ba atoms and $-0.036e$ on the six second-nearest-neighbour fluorine atoms. According to the results of our calculations, the experimentally measurable F centre spin density is equal to $0.747e$ (see table 3). Unfortunately, we did not find the experimental data for the F centre spin density in BaF_2 in the literature.

The fluorine vacancy site (F centre) is surrounded in the ideal lattice by four Ba atoms forming a tetrahedron (see figure 5). The next-nearest-neighbour shell is formed by six fluorine atoms. The positions of 10 atoms surrounding the F centre in BaF_2 with point group symmetry T_d after lattice relaxation to the minimum of the total energy are calculated by means of the B3PW method. The conclusion is that the repulsions of the four nearest Ba atoms from the F centre by 0.03% a_o and inward displacements of the second-nearest-neighbour F atoms by 0.23% a_o are small, since the effective charge of the F centre is close to the effective charge of

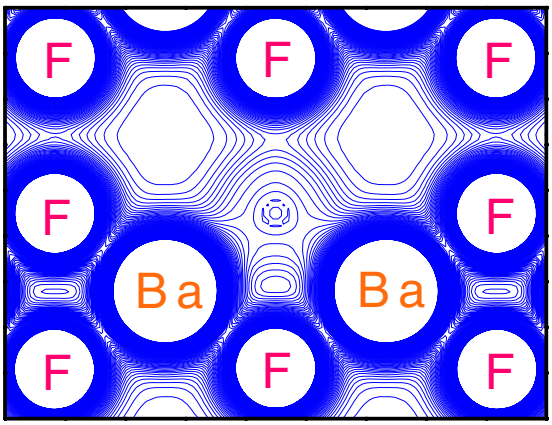

Figure 4. Charge density map of BaF_2 with F centre from the (110) side view. Isodensity curves are drawn from 0 to 0.1 e/bohr^3 with an increment of 0.001 e/bohr^3.

Table 3. The effective charges ($Q(e)$) of the F centre and surrounding atoms in the BaF_2 bulk calculated by the hybrid B3PW method for a supercell containing 48 atoms. ΔQ (e) is the charge difference between the defective and perfect BaF_2 crystal.

Atom (ith nearest)	Q (e)	ΔQ (e)	Spin (n_α–n_β) (e)
XX	−0.801	+0.122	0.747
Ba(1)	+1.828	−0.017	0.045
F(2)	−0.929	−0.006	0.008
F(3)	−0.923	0	0
Ba(4)	+1.845	0	0

the fluorine atom. We found that the defect–defect coupling due to the periodically repeated defects in our supercell model is negligible for the 48-atom supercell, since the width of the defect band is only 0.016 eV.

As mentioned in the introduction, BaF_2 exhibits optical absorption, centred around 2.3 eV [4]. Our results for defect levels (see figure 6) suggest a possible mechanism for this optical absorption. In the ground state, the defect band is occupied in the α graph and unoccupied in the β figure (see figure 6). The optical absorption corresponds to an electron transition from the F-centre ground state to the conduction band. Because of the spin difference between α and β states and the selection rules, the electron transition from the α occupied band to the β unoccupied band is impossible. The experimentally observed optical absorption could be due to an electron transfer from the F-centre ground state, located at the Γ point 7.01 eV above the valence band top to the conduction band bottom. The corresponding calculated value is 4.27 eV, which, however, still differs considerably from the experimental result. This discrepancy may be caused by the reason that we calculated the optical absorption energy as a difference between occupied and unoccupied one-electron energies, which in general is a very crude approximation, but could be justified in our case by the fact that we have excellent agreement between the experimental and our calculated band gap.

The presence of an unpaired electron is also revealed by the band structure of the defective system, given in figure 6. The bound unpaired electron level lies in the gap; the corresponding unoccupied level appears in the β spin structure, again in the gap but at positive energies. Unlike unpolarized band structure curves whose states can be occupied by two electrons, only one electron occupies one state in figure 6.

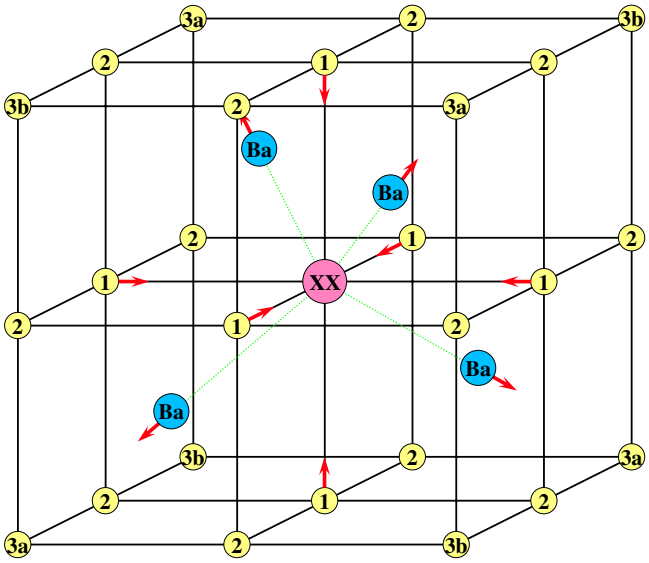

Figure 5. A view of the F-centre nearest-neighbour geometry in BaF_2 with the indication of relaxation shifts. The position of the colour centre is indicated by XX. The fluorines are labelled 1 in the first shell, 2 in the second shell and 3a and 3b in the third shell.

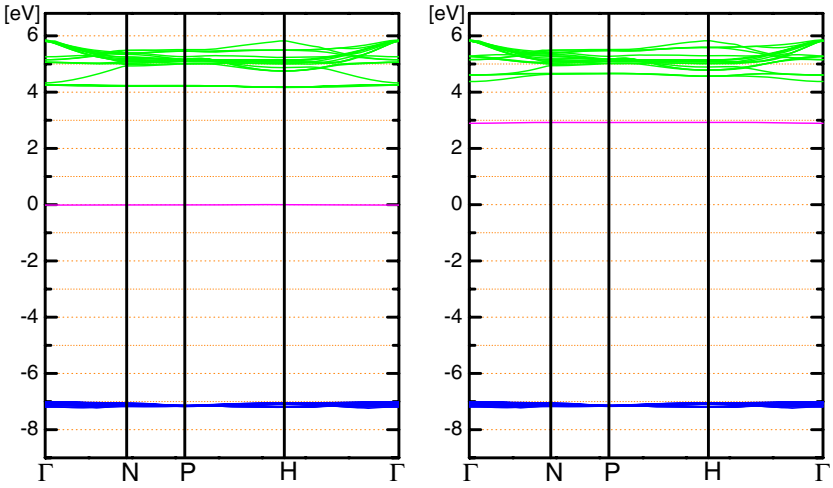

Figure 6. Calculated band structure for the 48-atom supercell modelling the F centre in BaF_2. α (left) and β (right) denote the majority and minority spin states, respectively.

A hyperfine structure of the EPR spectra can be detected, due to the interaction between the unpaired spin and the spin of neighbouring nuclei. This information gives better insight into the structure of the defect. The isotropic hyperfine interaction is caused by the non-zero probability of an electron being in the position of a given nucleus. This is only true for the s-type orbitals (they are the only ones which do not become zero at the origin). The anisotropic contribution is due to the presence of higher-order poles, and it is indicative of the deformation of the electronic density with respect to the spherical distribution.

The electron and nuclear spin coupling term $\mathcal{H}_S$ in the Hamiltonian is defined as:

$$\mathcal{H}_S = \tilde{\mathbf{S}} \cdot \mathbf{A} \cdot \mathbf{N} \tag{3}$$

where $\mathbf{S}$ and $\mathbf{N}$ denote the electron and the nuclear spin vector operators, respectively, $\tilde{\mathbf{S}}$ is the transpose of $\mathbf{S}$, and $\mathbf{A}$ is known as the hyperfine parameter matrix. The symmetry properties of $\mathbf{A}$ allow its decomposition into two terms as follows:

$$\mathbf{A} = A_0 \mathbf{I_3} + \mathbf{T} \tag{4}$$

$\mathbf{T}$ being a traceless tensor, $\mathbf{I_3}$ a 3×3 identity matrix and A_0 a scalar quantity. Thus, substituting (4) into (3), $\mathcal{H}_S$ can be written as the sum of an isotropic (iso) and an anisotropic or dipolar (dip) component:

$$\mathcal{H}_S = \mathcal{H}_{\text{iso}} + \mathcal{H}_{\text{dip}} \tag{5}$$

with

$$\mathcal{H}_{\text{iso}} = A_0 \tilde{\mathbf{S}} \cdot \mathbf{N} \tag{6}$$

and

$$\mathcal{H}_{\text{dip}} = \tilde{\mathbf{S}} \cdot \mathbf{T} \cdot \mathbf{N} = -\frac{\mu_0}{4\pi} g \beta_e g_N \beta_n \left(\frac{\tilde{\mathbf{S}} \cdot \mathbf{N}}{r^3} - \frac{3\tilde{\mathbf{S}} \cdot \mathbf{r}\, \mathbf{N} \cdot \mathbf{r}}{r^5} \right). \tag{7}$$

Usually, the experimental hyperfine coupling data are reported in terms of the isotropic a and anisotropic b hyperfine coupling constants. For each nucleus N, they (in MHz) are expressed as [32]

$$a = \frac{2\mu_0}{3h} g \beta_e g_N \beta_n \rho^{\alpha-\beta}(0) \tag{8}$$

$$b = \frac{\mu_0}{4\pi h} g \beta_e g_N \beta_n \left[T_{11} - \frac{1}{2}(T_{22} + T_{33}) \right] \tag{9}$$

where the spin density $\rho^{\alpha-\beta}$ at N, the elements of the hyperfine coupling tensor $\mathbf{T}$, and the electron g factor are the only terms that depend on the electronic structure of the system. All other multiplicative factors in (7)–(9) are tabulated constants [32, 33] (h is the Planck constant, β_e and β_n are the electronic and nuclear magnetons, μ_0 is the permeability of the vacuum, and g_N is the nuclear g factor). $\mathbf{T}$ is a tensor of rank 2, which is obtained as the field gradient of the spin density at N. Its generic element has the form:

$$T_{ij}^N = \sum_{\mu\nu} \sum_{\mathbf{G}} P_{\mu\nu\mathbf{G}}^{\text{spin}} \int \varphi_\mu(\mathbf{r}) \left(\frac{r^2 \delta_{ij} - 3 r_i r_j}{r^5} \right) \varphi_\nu(\mathbf{r} - \mathbf{G})\, \mathrm{d}\mathbf{r} \tag{10}$$

where the origin of the Cartesian reference system is at nucleus N, r_i denotes the ith component of $\mathbf{r}$, and $\varphi_\nu(\mathbf{r} - \mathbf{G})$ is the νth atomic orbital centred in cell $\mathbf{G}$. $P_{\mu\nu\mathbf{G}}^{\text{spin}}$ is the direct space spin density matrix element connecting the μth atomic orbital in the zero cell (the reference cell) to the νth one in cell $\mathbf{G}$.

The calculated and experimental values of a for the coupling of the unpaired electron spin to nuclear spins are presented in table 4. For F(1), our calculation underestimates the experimental value by nearly 45%, but it is better than other theoretical results [11, 34]. The evaluation of F(3a) is in good agreement with experiment, but F(2) and F(3b) are underestimated considerably.

A comparison of our B3PW calculation for the anisotropic hyperfine constants b with other theoretical studies and experimental results [11] is also presented in table 4. The agreement for b constants is much better than for a. From table 4, we find it difficult to give good theoretical results for hyperfine constants, unlike the lattice constant, bulk modulus and band gaps. However, on the whole, our results for hyperfine coupling look quite reasonable.

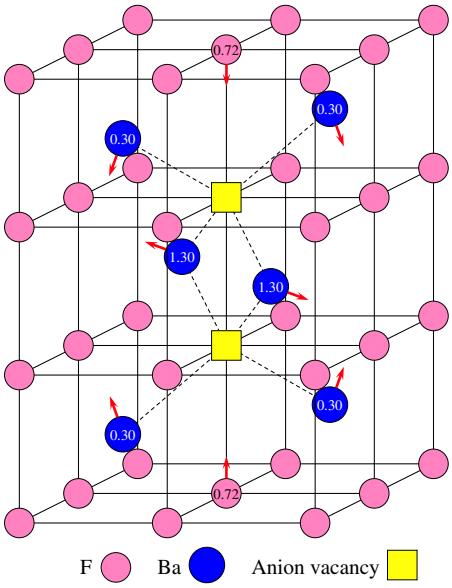

Figure 7. A view of the M-centre nearest-neighbour geometry in BaF_2 with indication of relaxation shifts. The positions of the anion vacancies are indicated by two squares. The directions of atomic displacements are shown with arrows; the values are given as a percentage of the lattice constant.

Table 4. Observed and calculated isotropic hyperfine constants a and b (MHz) for the F centre in BaF_2.

Atom (*shell*) (a)	Our results	Experiment [11]	Theory [11]	Theory [34]
F(1)	29.46	53.8	149.0	174.70
F(2)	0.66	5.1	7.7	23.09
F(3a)	46.38	42.6	0.89	28.52
F(3b)	0.09	2.2	0.89	1.20
Atom (*shell*) (b)	Our results	Experiment [11]	Theory [11]	
F(1)	6.59	7.0	15.5	
F(2)	0.51	1.1	1.45	
F(3a)	6.00	5.4	0.55	
F(3b)	0.36	0.5	0.55	

5. M centre in BaF_2

F centres in additively coloured alkaline earth fluoride crystals readily aggregate, forming more complex centres [35]. The simplest aggregate, the M centre (see figure 7), is composed of two F centres. We computed a 96-atom supercell with two of the neighbour fluorine atoms removed.

The redistribution of the electrons after M-centre formation was calculated using the hybrid B3PW method (see figure 8). The effective charges of the anion vacancies in this M-centre case are $-0.794e$ and increase slightly by $0.007e$ in comparison with the F-centre case. Bond population analysis between vacancy–vacancy ($+142me$) in the M-centre system and the F–F bond ($-2me$) in perfect BaF_2 bulk shows that the major effect observed here is a considerable covalency.

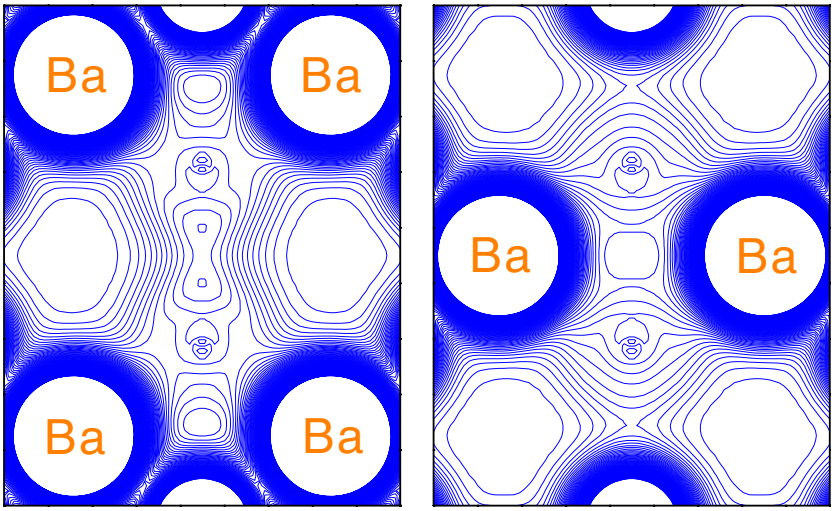

Figure 8. Charge density map of a BaF_2 crystal with the periodic M centre from the (1 1 0) (left) and (1 $\bar{1}$ 0) (right) side view. Isodensity curves are drawn from 0 to 0.1 e/bohr^3 with an increment of 0.001 e/bohr^3.

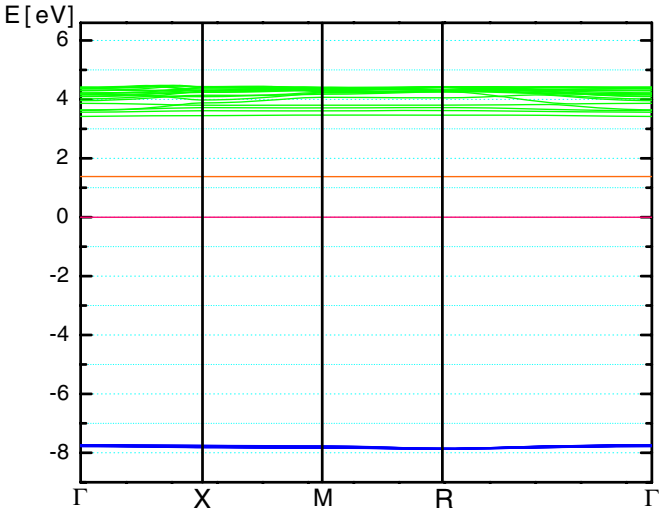

Figure 9. Calculated band structure for the 96-atom supercell modelling the M centres in BaF_2.

The β band absorption is predominantly due to the presence of M centres [35]. In the M-centre case, the α band is occupied by two electrons, so the electron transition from the α band to the β band is possible. M centres contribute to absorption in the β band, and this band will sometimes be referred to as the M band. Our calculation of the direct optical gap ($\Gamma \rightarrow \Gamma$) for M centres in BaF_2 is 1.38 eV and is much smaller than the corresponding value in the F-centre case (4.27 eV) (see figure 9). A similar phenomenon, a decrease in the optical gap for M centres, was also observed for CaF_2 and SrF_2 [35]. Compared with figure 6, the α band moves upward (toward the gap) (Γ point) by 0.74 eV, whereas the β band shifts downward by 0.55 eV.

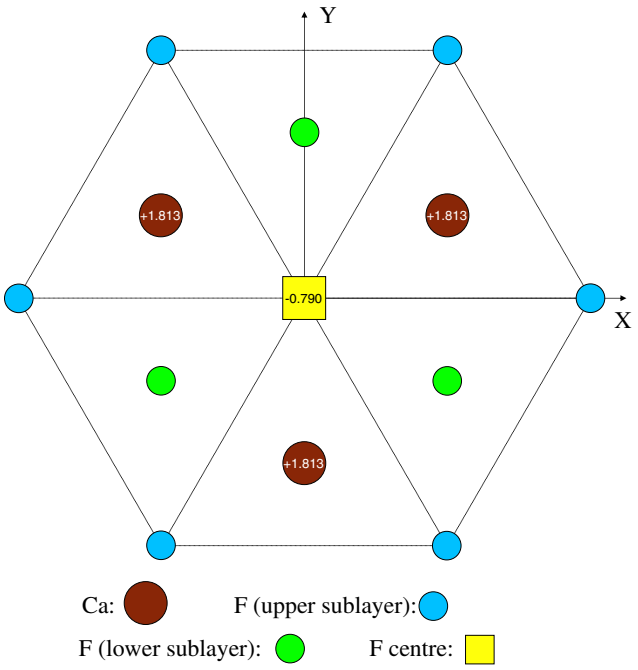

Figure 10. A top view of the surface F-centre nearest-neighbour geometry with the indication of effective charges.

6. Surface F centres in BaF_2

As an extension of our study dealing with F centres in BaF_2 bulk, we performed calculations for BaF_2 surface F centres. The atomic and electronic structure of surface F centres in BaF_2 is practically unknown, and according to our knowledge has never been addressed in the literature.

In the present work, we have studied the surface F centres on the $BaF_2(111)$ surface, which is the most stable surface according to our previous discussion about the pure BaF_2 slabs. We performed our surface F centre investigations for a slab containing four layers. Each layer consists of three sublayers, containing nine atoms. Therefore, we performed the surface F centre calculations for supercells containing 108 atoms.

According to the results of our calculations, the formation energy for the surface F centre located in the top layer was found to be 7.48 eV. The conclusion can be drawn that the defect formation in the $BaF_2(111)$ surface is 0.34 eV smaller than in the bulk. This is similar to what has been obtained for other materials and is due to the reduced coordination at the surface [36]. The lower formation energy for a surface F centre shows the preference for F centres located near the surface.

The relaxation of the atoms nearest to the surface F centre is calculated. Unlike the slight repulsion in the bulk F centre case, the nearest three Ba atoms located in the second sublayer of the top surface layer approach the surface F centre by 0.13% a_0. The three neighbouring F atoms located in the third sublayer of the first surface layer are attracted to the surface F centre by 0.37% a_0. The magnitude of this displacement is larger than that in the bulk F centre case (0.23%) by around 60%.

With respect to the electronic structure of the surface F centre in BaF_2, the effective charge analysis shows that the electronic density around it is slightly more delocalized than that corresponding to the bulk F centre. Figure 10 shows the top view of the surface F centre

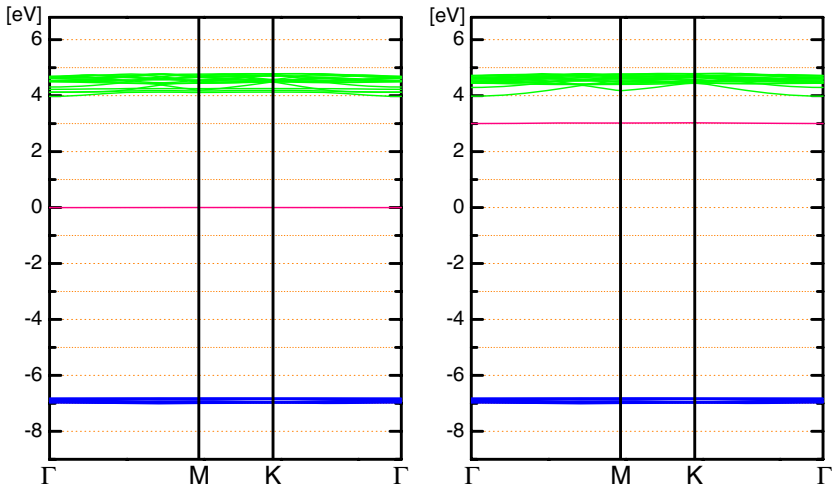

Figure 11. Calculated band structure for the 108-atom supercell modelling the surface F centre in BaF_2. α (left) and β (right) denote the majority and minority spin states, respectively.

configuration in BaF_2 and the effective charge values of the F centre and the nearest Ba atoms. The effective charge localized inside the surface F centre in BaF_2 is $-0.790e$, $0.011e$ less than for the bulk F centre ($-0.801e$) in BaF_2 (see table 3). The charges of the nearest Ba atoms of the surface F centre ($+1.813e$) are reduced by 0.015 e in comparison with the charges of the respective Ba atoms ($+1.828e$) near the bulk F centre. Bond populations between the surface F centre and the nearest Ba atoms are calculated. The major effect observed here is a strengthening of the surface F centre and Ba chemical bond. The surface F centre–Ba bond population is $28me$, which is larger than the relevant value in the bulk by $10me$. A similar but stronger effect, strengthening of the Ti–O chemical bond near the surface, was observed earlier also for $SrTiO_3$ [37, 38].

The α energy band corresponding to the surface F centre at Γ point is located 6.83 eV (0.18 eV lower than in the bulk F-centre case) above the valence band top and is separated from the conduction band bottom by 3.98 eV (see figure 11). Because of the surface effect, this gap is smaller than the corresponding value in the bulk F-centre case (4.27 eV). On the other hand, the β band is located 9.83 eV above the valence band top and shifts downward by 0.08 eV with respect to the bulk F-centre case. The negligible dispersion effect of the defect band for a 108-atom supercell means that the defect–defect interaction is practically eliminated, thus approaching the desired isolated single F centre limit.

7. Conclusions

It is well known that the Hartree–Fock calculation usually overestimates the band gap by a factor of two, whereas methods based on density functional theory considerably underestimate it. In order to solve this problem, we demonstrate that it is possible to achieve the best agreement with experiment (11.00 eV) by means of the hybrid B3PW method (11.30 eV).

The direct band gap for BaF_2 bulk (11.30 eV) is narrowed for the (111) (10.94 eV), (110) (10.77 eV) and (100) (10.29 eV) surfaces. This is in line with our previous study of ABO_3 [15] perovskites, where the (100) surface band gap was also narrowed with respect to the bulk. The BaF_2(111) surface energy, according to our calculations, is the smallest one

(0.334 J m^{-2}), indicating that the (111) surface is the most stable one, and more stable than CaF_2(111) surface [17].

According to our calculations, the relaxation of F atoms in the upper sublayer of the top (111) surface layer is inwards by 0.054 Å, and is comparable with the LEED experiment (0.12 ± 0.07 Å) [28]. The surface-layer relaxation of atoms in the BaF_2 upper sublayer has the same direction and comparable magnitude as we found earlier for CaF_2 [17].

The analysis of the effective charges shows that the electron associated with the removed F atom is well localized inside the fluorine vacancy. The relaxation of the atoms surrounding the F centre according to our calculations is small. The creation of a neutral fluorine vacancy in BaF_2 results in a new F-centre defect band located at the Γ point 7.01 eV above the valence band top. We suggest that the optical absorption energy, experimentally observed in BaF_2 crystal at around 2.3 eV, can be due to electron transfer from the F-centre ground state to the conduction band. Our calculations of hyperfine coupling constants are in qualitative agreement with experimental results.

The β band absorption is predominantly due to the presence of M centres. According to our calculations, the direct optical gap ($\Gamma \rightarrow \Gamma$) for M centres in BaF_2 is 1.38 eV and is much smaller than the corresponding value in the F-centre case.

The formation energy for the surface F centre in BaF_2 (7.48 eV) is 0.34 eV smaller than in the bulk and implicates the trend for F centres to locate near the surface.

References

[1] Schmidt E D and Vedam K 1966 *J. Phys. Chem. Solids* **27** 1563
[2] Dutt N, Sharma O P and Shanker J 1985 *Phys. Status Solidi* **127** 67
[3] Kudrnovsky J, Christensen N E and Masek J 1991 *Phys. Rev.* B **43** 12597
[4] Nepomnyashchikh I, Radzabov E A, Egranov A V, Ivasheckin V F and Istomin A S 2002 *Radiat. Eff. Defects Solids* **157** 715
[5] Khenata R, Daoudi B, Sahnoun M, Baltache H, Rerat M, Reshak A H, Bouhafs B, Abid H and Driz M 2005 *Eur. Phys. J.* B **47** 63
[6] Rubloff G W 1972 *Phys. Rev.* B **5** 662
[7] Kawano K *et al* 1999 *Phys. Rev.* B **60** 11984
[8] Sata N, Eberman K, Eberl K and Maier J 2000 *Nature* **408** 946
[9] Arends J 1964 *Phys. Status Solidi* **7** 805
[10] Hayes W and Stott J P 1967 *Proc. R. Soc.* A **301** 313
[11] Stoneham A M, Hayes W, Smith P H S and Stott J P 1968 *Proc. R. Soc.* A **306** 369
[12] Vail J M, Coish W A, He H and Yang A 2002 *Phys. Rev.* B **66** 014109
[13] Saunders V R, Dovesi R, Roetti C, Causa M, Harrison N M, Orlando R and Zicovich-Wilson C M 2003 *CRYSTAL-2003 User Manual* (Italy: University of Torino)
[14] Piskunov S, Heifets E, Eglitis R I and Borstel G 2004 *Comput. Mater. Sci.* **29** 165
[15] Eglitis R I, Piskunov S, Heifets E, Kotomin E A and Borstel G 2004 *Ceram. Int.* **30** 1989
[16] Hay P J and Wadt W R 1984 *J. Chem. Phys.* **82** 299
[17] Shi H, Eglitis R I and Borstel G 2005 *Phys. Rev.* B **72** 045109
[18] Becke A D 1993 *J. Chem. Phys.* **98** 5648
[19] Perdew J P and Wang Y 1986 *Phys. Rev.* B **33** 8800
[20] Perdew J P and Wang Y 1989 *Phys. Rev.* B **40** 3399
[21] Perdew J P and Wang Y 1992 *Phys. Rev.* B **45** 13244
[22] Monkhorst H J and Pack J D 1976 *Phys. Rev.* B **13** 5188
[23] Padilla J and Vanderbilt D 1998 *Surf. Sci.* **418** 64
[24] Cheng C, Kunc K and Lee M H 2000 *Phys. Rev.* B **62** 10409
[25] Sousa C and Illas F 2001 *J. Chem. Phys.* **115** 1435
[26] Leger J M, Haines J, Atouf A and Schulte O 1995 *Phys. Rev.* B **52** 13247
[27] Muscat J, Wander A and Harisson N M 2001 *Chem. Phys. Lett.* **342** 397
[28] Vogt J, Henning J and Weiss H 2005 *Surf. Sci.* **578** 57
[29] Zhang S B and Northrup J E 1991 *Phys. Rev. Lett.* **67** 2339

[30] Mattila T, Poykko S and Nieminen R M 1997 *Phys. Rev.* B **56** 15665
[31] Mallia G, Orlando R, Roetti C, Ugliengo P and Dovesi R 2001 *Phys. Rev.* B **63** 235102
[32] Weil J A, Bolton J R and Wertz J E 1994 *Electron Paramagnetic Resonance* (New York: Wiley)
[33] Lide D (ed) 1992 *Handbook of Chemistry and Physics* 72nd edn (Boston: CRC Press) pp 1991–2
[34] Bartram R H, Harmer A L and Hayes W 1971 *J. Phys. C: Solid State Phys.* **4** 1665
[35] Hayes W 1974 *Crystals with the Fluorite Structure* (Oxford: Clarendon)
[36] Carrasco J, Gomes J R B and Illas F 2004 *Phys. Rev.* B **69** 064116
[37] Heifets E, Eglitis R I, Kotomin E A, Maier J and Borstel G 2001 *Phys. Rev.* B **64** 235417
[38] Heifets E, Goddard W A III, Kotomin E A, Eglitis R I and Borstel G 2004 *Phys. Rev.* B **69** 035408